



Initial results for the north pole of the Moon from Mini-SAR, Chandrayaan-1 mission

P. D. Spudis,¹ D. B. J. Bussey,² S. M. Baloga,³ B. J. Butler,⁴ D. Carl,² L. M. Carter,⁵ M. Chakraborty,⁶ R. C. Elphic,⁷ J. J. Gillis-Davis,⁸ J. N. Goswami,⁹ E. Heggy,¹⁰ M. Hillyard,² R. Jensen,² R. L. Kirk,¹¹ D. LaVallee,² P. McKerracher,² C. D. Neish,² S. Nozette,¹ S. Nylund,² M. Palsetia,¹² W. Patterson,² M. S. Robinson,¹³ R. K. Raney,² R. C. Schulze,² H. Sequeira,² J. Skura,² T. W. Thompson,¹⁰ B. J. Thomson,² E. A. Ustinov,¹⁰ and H. L. Winters²

Received 22 December 2009; revised 10 February 2010; accepted 22 February 2010; published 31 March 2010.

[1] We present new polarimetric radar data for the surface of the north pole of the Moon acquired with the Mini-SAR experiment onboard India's Chandrayaan-1 spacecraft. Between mid-February and mid-April, 2009, Mini-SAR mapped more than 95% of the areas polewards of 80° latitude at a resolution of 150 meters. The north polar region displays backscatter properties typical for the Moon, with circular polarization ratio (CPR) values in the range of 0.1–0.3, increasing to over 1.0 for young primary impact craters. These higher CPR values likely reflect surface roughness associated with these fresh features. In contrast, some craters in this region show elevated CPR in their interiors, but not exterior to their rims. Almost all of these features are in permanent sun shadow and correlate with proposed locations of polar ice modeled on the basis of Lunar Prospector neutron data. These relations are consistent with deposits of water ice in these craters. **Citation:** Spudis, P. D., et al. (2010), Initial results for the north pole of the Moon from Mini-SAR, Chandrayaan-1 mission, *Geophys. Res. Lett.*, 37, L06204, doi:10.1029/2009GL042259.

1. Introduction

[2] Volatiles deposited on the Moon by cometary and asteroidal impacts and the continuous impingement of solar wind hydrogen might migrate to and collect in permanently

shadowed cold traps near the lunar poles, where they would be stable over geologic time [Arnold, 1979]. Because these cold traps receive no direct solar illumination, and emit little radiation, most are difficult to observe from the Earth. Radar can identify deposits of frozen volatiles because under certain conditions, they produce a unique backscatter signature. A high (>1.0) ratio of same sense to opposite sense polarization and high reflectivity has been detected by radar on the Galilean satellites of Jupiter [Hapke, 1990; Ostro and Shoemaker, 1990], the residual south polar ice cap of Mars [Muhleman et al., 1991] and the inside of permanently shadowed polar craters on Mercury [Harmon and Slade, 1992; Butler et al., 1993]. These characteristics are attributed to multiple internal reflection and/or coherent backscatter produced by low-loss material, such as water ice [Ostro and Shoemaker, 1990].

[3] Circular Polarization Ratio (CPR) is the ratio of power of the received signal in the same sense (SC; same sense circular) to that of the opposite sense (OC; opposite sense circular) as transmitted (SC/OC). Typically, rocky planets have low CPR (between 0.2 and 0.4), except for surfaces that are very rough on wavelength scales, in which CPR is elevated (caused by multiple double-bounce reflections). Ice is transparent to RF energy and radar is multiply scattered by imperfections and inclusions in the ice, also resulting in high CPR. The Clementine bistatic radar experiment [Nozette et al., 1996, 1997, 2001] revealed elevated CPR in the south polar region at bistatic angles close to zero, suggesting the presence of patchy ice deposits in the permanently dark areas of Shackleton crater. Later studies questioned this interpretation [e.g., Stacy et al., 1997; Campbell et al., 2006] and suggested that high CPR observed by Arecibo near the south pole are caused by surface roughness alone as only some of these areas are permanently shadowed. However, the presence of surface scatters in sunlight does not preclude the possibility of volume scattering ice in permanent darkness [Nozette et al., 2001]. Independently, the neutron spectrometer on the Lunar Prospector mission measured low epithermal neutron flux at both poles, indicating elevated amounts of near-surface hydrogen near the poles [Feldman et al., 1998, 2000]. Combined with study of permanently shadowed areas [Margot et al., 1999], the neutron signal has been attributed to the presence of water ice in dark polar craters [Lawrence et al., 2006; Elphic et al., 2007].

[4] Mini-SAR is an S-band ($\lambda = 12.6$ cm) imaging radar designed to map the polar terrain and to collect information

¹Lunar and Planetary Institute, Houston, Texas, USA.

²Johns Hopkins University Applied Physics Laboratory, Laurel, Maryland, USA.

³Proxemy Research Inc., Laytonville, Maryland, USA.

⁴National Radio Astronomy Observatory, Socorro, New Mexico, USA.

⁵Center for Earth and Planetary Studies, Smithsonian Institution, Washington, D.C., USA.

⁶Space Applications Centre, ISRO, Ahmedabad, India.

⁷NASA Ames Research Center, Moffett Field, California, USA.

⁸Hawaii Institute of Geophysics and Planetology, University of Hawaii, Honolulu, Hawaii, USA.

⁹Physical Research Laboratory, Ahmedabad, India.

¹⁰Jet Propulsion Laboratory, Pasadena, California, USA.

¹¹Astrogeology Program, U. S. Geological Survey, Flagstaff, Arizona, USA.

¹²Vexcel Inc., Boulder, Colorado, USA.

¹³School of Earth and Space Exploration, Arizona State University, Tempe, Arizona, USA.

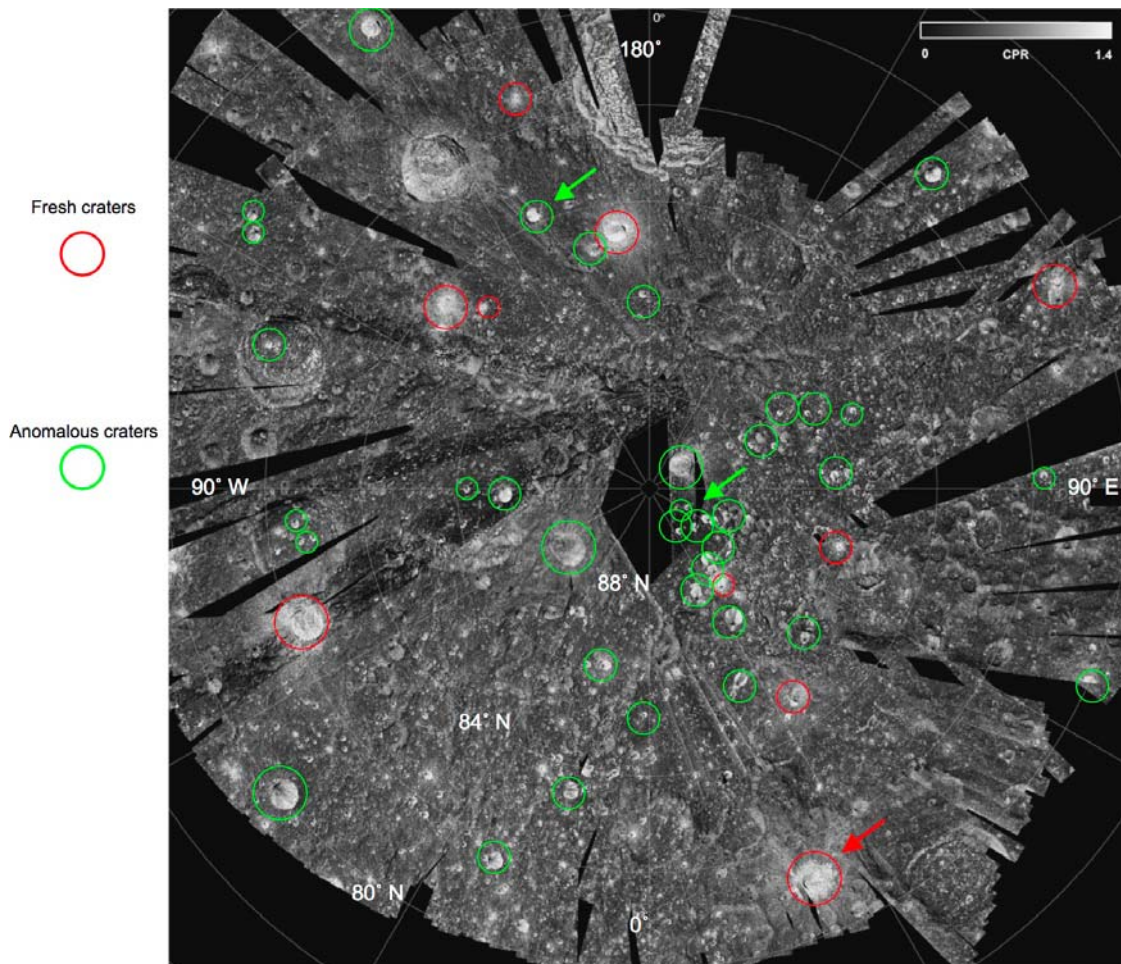


Figure 1. CPR map of the north polar region of the Moon. Normal appearing fresh craters are indicated by red circles while anomalous craters having high CPR in their interiors are shown by green circles. Although both crater types are found throughout the map area, anomalous craters (green) are concentrated at the higher latitudes and have at least some portion of their floors in permanent shadow. The red arrow points to Main L (Figure 2); the green arrow is the crater shown in Figure 3.

about the scattering properties of illuminated and permanently dark areas of the lunar poles near optimum (45°) viewing geometry [Spudis *et al.*, 2009]. From February to April 2009, the Chandrayaan-1 Mini-SAR mapped over 95% of the lunar poles (latitude $> 80^\circ$) at 150 m radar resolution. The instrument utilizes a hybrid polarity architecture [Raney, 2007] which transmits circular polarization and receives two orthogonal linear polarizations coherently. This configuration allows us to reconstruct the four Stokes parameters of the backscattered field that are equivalent to those which would be measured by a conventional radar astronomical telescope that transmitted and received exclusively in circular polarizations.

2. Results

[5] The average CPR of the lunar surface is on the order of 0.2 to 0.4 at 45° incidence for typical terrains [Campbell *et al.*, 2006; Thompson *et al.*, 2008; Carter *et al.*, 2009]. The north polar region displays many areas of elevated CPR (Figure 1). In some cases, this enhancement is clearly associated with morphologically fresh, young impact craters

(red circles; Figure 1). This phenomenon is well known; the youngest features on the Moon are the roughest, with newly formed craters excavating large quantities of ejecta, having impact melt sheets with roughly textured flow surfaces and cracks, and throwing out many angular blocks [Schultz, 1976; Wilhelms, 1987; Heiken *et al.*, 1991]. High CPR is found both within and outside of such features (red circles; Figure 1); high-resolution images of sunlit, fresh impact craters indicate a high degree of wavelength-scale surface roughness both within and outside the crater's rims [Schultz, 1976]. As features degrade and weather with time, the micrometeorite bombardment of the Moon slowly grinds rocks and small-scale textures into powder, gradually erasing the rough surface signature of fresh craters [Schultz, 1976; Wilhelms, 1987; Heiken *et al.*, 1991] and merging the craters into the low CPR background of the lunar surface. These processes are continuous, cumulative, and progressive.

[6] The crater Main L (81.2°N , 22.7°E ; 14 km diameter) is illuminated by sunlight both inside and outside its rim over the course of a lunar day. It is a fresh, Copernican-age impact crater and hence, is expected to display youthful

Fresh crater

Main L, 14 km diameter, 81.4° N, 22° E

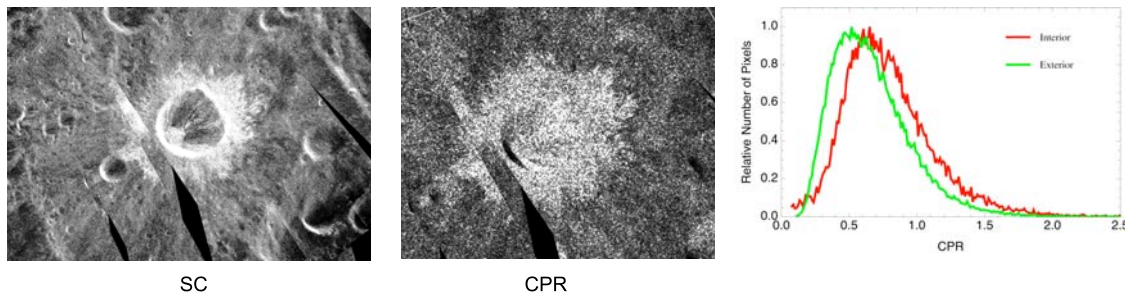


Figure 2. Example of a fresh impact crater, Main L (14 km diameter; 81.2°N, 22.7°E). The Copernican-age crater displays high radar backscatter and elevated CPR, which occurs both within and outside the rim of the feature (histogram). Such a distribution is consistent with high CPR caused by enhanced degrees of wavelength-scale surface roughness. The relative youth of Main L results in abundant blocks and small-scale surface roughness associated with ejecta deposits inside and outside of the crater.

morphological attributes, including many angular blocks and enhanced surface roughness in its interior and exterior. Mini-SAR images of this feature (Figure 2) confirm these expectations; the crater shows high radar backscatter in the SAR image and elevated CPR, both inside and outside of the crater rim (Figure 2). Main L is in all respects a typical young impact crater and the CPR patterns revealed by our mapping can be used to infer high degrees of small-scale

surface roughness in its deposits, both interior and exterior to the rim.

[7] Several craters found near the north pole of the Moon show a different pattern (Figures 1 and 3). While most of the floor of the crater Rozhdestvensky (85.2 N, 155.4 W; 177 km diameter) is not in permanent darkness, the interiors of small (5–15 km diameter) craters found on its floor are [Margot et al., 1999; Bussey et al., 2005; Noda et al., 2008].

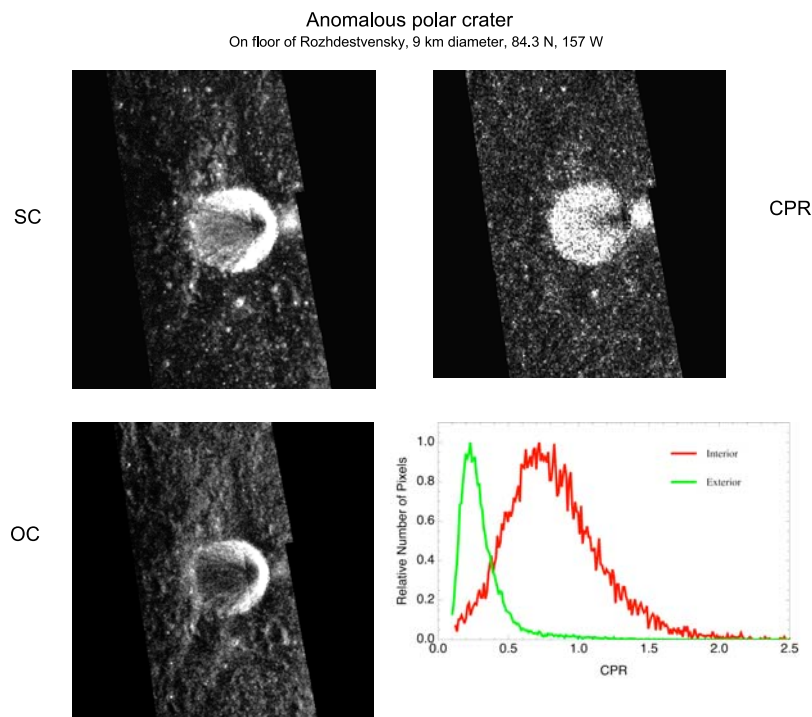


Figure 3. Small polar anomalous crater (83.8°N, 157.1°W; 8 km diameter) on the floor of the large crater Rozhdestvensky (85.2 N, 155.4 W; 177 km diameter). Clockwise from upper left are the same-sense circular image (SC), CPR, CPR histogram, and the opposite sense circular (OC) images. Elevated CPR is found inside but not outside the crater rim; this crater interior is in permanent shadow [Noda et al., 2008]. Note the enhanced returns in the SC, OC and CPR images compared to the crater near Byrgius (Figure 4); these properties are consistent with volume scattering in this crater interior.

Table 1. Scattering Properties of Crater Materials Seen by Mini-SAR

Quantity	Main L Interior	Main L Exterior	Rozhdestvensky Interior	Rozhdestvensky Exterior	Byrgius Interior	Byrgius Exterior
CPR Geometric Mean $\pm \sigma$	0.71 \pm 0.32	0.66 \pm 0.28	0.74 \pm 0.32	0.28 \pm 0.17	1.01 \pm 0.36	0.57 \pm 0.21
Standard Skewness	15.81	33.47	5.93	47.55	20.47	19.79
Standard Kurtosis	8.75	22.51	0.78	76.71	16.45	13.96

An example is shown in Figure 3. This unnamed feature shows elevated CPR (mean value ~ 0.74) *within* the bounds of its rim, but *no* enhancement of CPR exterior to its rim (mean value ~ 0.28 ; Figure 3). This distribution is unlike that found around fresh craters such as Main L, where high CPR is associated with rough terrain in *both* the crater interior and exterior (Figure 2, Table 1).

[8] A geological process that results in high degrees of surface roughness within, but not outside, of a crater rim is difficult to envision. One possibility is that the initial distribution of surface roughness around the crater was asymmetric; such a relation might be caused during the formation of secondary craters from high-angle, low-velocity material [Heiken *et al.*, 1991], which might preserve debris within its rim crest, while excavating only smooth, local regolith. There is no indication that any of these craters are secondaries; no herringbone patterns, overlap or chaining of irregular craters are observed. Many craters of intermediate age on the Moon preserve outcrop just inside their rim crests, leading to parts of their interiors showing elevated CPR with lower values external to their rims [e.g., Campbell *et al.*, 2006]. However, the anomalous craters identified here display high CPR throughout the crater interior; it is not confined solely to the uppermost walls, associated with rock outcrop, or to the crater bottoms, a result of mass wasted debris [Wilhelms, 1987].

[9] Away-facing slopes alter the incidence angle of the radar waves and can increase apparent CPR values up to 50%, depending on the topography of the surface [Carter *et al.*, 2009]. Such an increase does not appear to be the sole cause of elevated CPR in the anomalous polar craters as the bowl-shaped craters (resulting in constantly changing incidence angles) show uniformly high CPR within the rim depression (Figures 1 and 3) and although a near-field rim slope effect is evident, CPR values are not arranged in conformity with the crater wall slopes throughout the interior of the feature. Over thirty craters in the north polar region show this anomalous pattern of CPR distribution (green circles; Figure 1). These craters have a wide variety of ages but all show elevated CPR confined within their rim crests. The anomalous craters are concentrated at high latitudes, especially on the flat floors of the larger craters Peary, Hermite, and Rozhdestvensky (green circles; Figures 1 and 3). Studies of lighting conditions near the north pole indicate that the interiors of these anomalous craters are permanently dark [Margot *et al.*, 1999; Bussey *et al.*, 2005; Noda *et al.*, 2008].

[10] Modeling of the thermal conditions of permanently dark areas near the poles [Vasavada *et al.*, 1999] indicates that they are significantly colder than 100 K; early data from the LRO Diviner experiment indicate cold trap temperatures as low as 25 K (D. A. Paige, Diviner observes extreme polar temperatures, 2009, available at <http://www.diviner.ucla.edu/blog/?p=232>).

At such temperatures, water ice and other volatiles are stable and once deposited in these cold traps and covered by a thin (few cm) layer of regolith are largely protected from processes of removal. As the Moon has been bombarded with water-bearing objects such as comets and meteorites and implanted with solar wind hydrogen over geological time, some of this material must have made its way into these cold, dark areas.

[11] Analyses of the CPR data for anomalous polar craters (Figure 1) reveal them to be unique. A few non-polar craters have been identified that also exhibit high interior and lower exterior CPR values; an example is near Byrgius A (5 km diameter, 21.2°S, 64.5°W; Figure 4). This crater displays a median CPR of about 1.0 inside and 0.6 outside its rim, a value nearly twice that found exterior to anomalous polar craters (Table 1). Unlike the polar craters, the crater near Byrgius shows relatively low SC backscatter (cf. Figures 3 and 4). While the CPR distributions of the interiors of both Main L and near Byrgius are highly peaked (high kurtosis), the distribution of CPR of the crater within Rozhdestvensky is dramatically flatter with a distinctly low kurtosis (Table 1). Skewness values of all the CPR distributions (Table 1) similarly suggest that the CPR population of the crater within Rozhdestvensky is different and distinct. Thus, although superficially similar, the high CPR of the anomalous polar craters likely has a different origin from those of both fresh and non-polar craters. The anomalous polar craters occur in close geographical association, with over 20 specific examples found within or near Peary (Figure 1) while the crater near Byrgius is isolated (Figure 4).

[12] The average CPR in the north polar area peaks around 0.29 (Figure 1), in accord with previous estimates for typical lunar surface [e.g., Carter *et al.*, 2009]. The polar anomalous craters show enhanced CPR in their interiors, with the crater in Rozhdestvensky showing a mean 0.74 ± 0.32 CPR with isolated values greater than 1.5 (Figure 3; Table 1). The elevated CPR, geological occurrence and setting of these features (confined within permanently shadowed polar areas) and low epithermal neutron flux (L. A. Teodoro, V. R. Eke, and R. C. Elphic, The spatial distribution of lunar polar hydrogen deposits after SELENE, 2009, available at <http://lunarscience2009.arc.nasa.gov/node/73>) are all consistent with the presence of water ice in these craters. The recent discovery of significant amounts of mobile water in the higher latitudes of the Moon [Pieters *et al.*, 2009] may provide one source for the polar ice inferred from these measurements. The Mini-SAR data show that ice is heterogeneously distributed within many (but not all) of the small craters near the north pole and must be at least tens of wavelengths ($\sim 2\text{--}3$ m) thick to create a volume-scattering CPR enhancement. Such a distribution could indicate an episodic, stochastic depositional history rather than a steady-state, equilibrium process. We plan to repeat our measure-

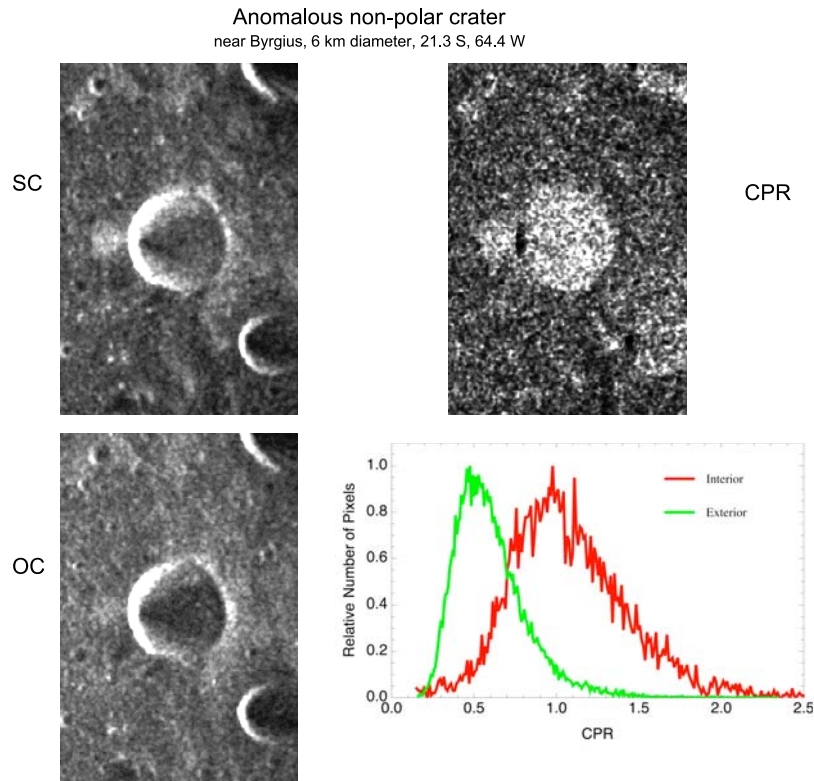


Figure 4. Small non-polar anomalous crater (21.2°S, 64.5°W; 5 km diameter) north of Byrgius (24.7°S, 65.3°W; 87 km diameter) displays high CPR in its interior but lower values outside its rim. Typical peak CPR values match both the Main L and polar anomalous examples, but SC returns are lower than the anomalous polar craters (Figure 3). Statistical analyses (Table 1) show that the distributions of CPR in this crater are similar to those of Main L (Figure 2) but not the polar anomalous craters (Figure 3). This crater interior is exposed to full sunlight over the course of a lunar day.

ments of these areas and observe new terrain using the Mini-RF experiment aboard NASA's Lunar Reconnaissance Orbiter to confirm and refine our estimates of the presence and distribution of ice at the poles of the Moon.

[13] **Acknowledgments.** We thank NASA's Space Operations Mission Directorate and Exploration Systems Mission Directorate, and the Department of Defense for supporting the Mini-SAR project. The instrument was built by Raytheon and BAE; project management was provided by the U. S. Navy's Air Warfare Center, China Lake CA. We thank the Indian Space Research Organization for selecting Mini-SAR for flight on Chandrayaan-1 and for supporting operations to obtain our mapping data. This paper is Lunar and Planetary Institute contribution 1540.

References

- Arnold, J. R. (1979), Ice in the lunar polar regions, *J. Geophys. Res.*, *84*, 5659–5668, doi:10.1029/JB084iB10p05659.
- Bussey, D. B. J., K. E. Fristad, P. M. Schenk, M. S. Robinson, and P. D. Spudis (2005), Constant illumination at the lunar north pole, *Nature*, *434*, 842, doi:10.1038/434842a.
- Butler, B. J., D. O. Muhleman, and M. A. Slade (1993), Mercury: Full-disk images and the detection and stability of ice at the north pole, *J. Geophys. Res.*, *98*, 15,003–15,023, doi:10.1029/93JE01581.
- Campbell, D. B., B. A. Campbell, L. M. Carter, J.-L. Margot, and N. J. S. Stacy (2006), No evidence for thick deposits of ice at the lunar south pole, *Nature*, *443*, 835–837, doi:10.1038/nature05167.
- Carter, L. M., B. A. Campbell, B. R. Hawke, D. B. Campbell, and M. C. Nolan (2009), Radar remote sensing of pyroclastic deposits in the southern Mare Serenitatis and Mare Vaporum regions of the Moon, *J. Geophys. Res.*, *114*, E11004, doi:10.1029/2009JE003406.
- Elphic, R. C., V. R. Eke, L. Teodoro, D. J. Lawrence, and D. B. J. Bussey (2007), Models of the distribution and abundance of hydrogen at the lunar south pole, *Geophys. Res. Lett.*, *34*, L13204, doi:10.1029/2007GL029954.
- Feldman, W. C., S. Maurice, A. B. Binder, B. L. Barraclough, R. C. Elphic, and D. J. Lawrence (1998), Fluxes of fast and epithermal neutrons from lunar prospector: Evidence for water ice at the lunar poles, *Science*, *281*, 1496–1500, doi:10.1126/science.281.5382.1496.
- Feldman, W. C., D. J. Lawrence, R. C. Elphic, B. L. Barraclough, S. Maurice, I. Genetay, and A. B. Binder (2000), Polar hydrogen deposits on the Moon, *J. Geophys. Res.*, *105*(E2), 4175–4195, doi:10.1029/1999JE001129.
- Hapke, B. (1990), Coherent backscatter and the radar characteristics of outer planet satellites, *Icarus*, *88*, 407–417, doi:10.1016/0019-1035(90)90091-M.
- Harmon, J. K., and M. A. Slade (1992), Radar mapping of Mercury: Full-disk Doppler delay images, *Science*, *258*, 640–643, doi:10.1126/science.258.5082.640.
- Heiken, G., D. Vaniman, and B. French (Eds.) (1991), *The Lunar Sourcebook: A User's Guide to the Moon*, 736 pp., Cambridge Univ. Press, Cambridge, U.K.
- Lawrence, D. J., W. C. Feldman, R. C. Elphic, J. J. Hagerty, S. Maurice, G. W. McKinney, and T. H. Prettyman (2006), Improved modeling of Lunar Prospector neutron spectrometer data: Implications for hydrogen deposits at the lunar poles, *J. Geophys. Res.*, *111*, E08001, doi:10.1029/2005JE002637.
- Margot, J. L., D. B. Campbell, R. F. Jurgens, and M. A. Slade (1999), Topography of the lunar poles from radar interferometry: A survey of cold trap locations, *Science*, *284*, 1658–1660, doi:10.1126/science.284.5420.1658.
- Muhleman, D. O., B. J. Butler, A. W. Grossman, and M. A. Slade (1991), Radar images of Mars, *Science*, *253*, 1508–1513, doi:10.1126/science.253.5027.1508.
- Noda, H., H. Araki, S. Goossens, Y. Isihara, K. Matsumoto, S. Tazawa, S. Sasaki, N. Kawano, and S. Sasaki (2008), Illumination conditions at the lunar polar regions by Kaguya (SELENE) laser altimeter, *Geophys. Res. Lett.*, *35*, L24203, doi:10.1029/2008GL035692.
- Nozette, S., C. Lichtenberg, P. D. Spudis, R. Bonner, W. Ort, E. Malaret, M. Robinson, and E. M. Shoemaker (1996), The Clementine bistatic

- radar experiment, *Science*, 274, 1495–1498, doi:10.1126/science.274.5292.1495.
- Nozette, S., E. M. Shoemaker, P. D. Spudis, and C. L. Lichtenberg (1997), The possibility of ice on the Moon, *Science*, 278, 144–145, doi:10.1126/science.278.5335.144.
- Nozette, S., P. D. Spudis, M. Robinson, D. B. J. Bussey, C. Lichtenberg, and R. Bonner (2001), Integration of lunar polar remote-sensing data sets: Evidence for ice at the lunar south pole, *J. Geophys. Res.*, 106(E10), 23,253–23,266, doi:10.1029/2000JE001417.
- Ostro, S. J., and E. M. Shoemaker (1990), The extraordinary radar echoes from Europa, Ganymede, and Callisto: A geological perspective, *Icarus*, 85, 335–345, doi:10.1016/0019-1035(90)90121-O.
- Pieters, C., et al. (2009), Character and Spatial Distribution of OH/H₂O on the Surface of the Moon Seen by M³ on Chandrayaan-1, *Science*, 326, 568–572, doi:10.1126/science.1178658.
- Raney, R. K. (2007), Hybrid-polarity SAR architecture, *IEEE Trans. Geosci. Remote Sens.*, 45, 3397–3404, doi:10.1109/TGRS.2007.895883.
- Schultz, P. H. (1976), *Moon Morphology*, pp. 182–185, Univ. Texas Press, Austin, Tex.
- Spudis, P., S. Nozette, B. Bussey, K. Raney, H. Winters, C. L. Lichtenberg, W. M. Marinelli, J. C. Crusan, and M. M. Gates (2009), Mini-SAR: An imaging radar experiment for the Chandrayaan-1 mission to the Moon, *Curr. Sci.*, 96, 533–539.
- Stacy, N. J. S., D. B. Campbell, and P. G. Ford (1997), Arecibo radar mapping of the lunar poles: A search for ice deposits, *Science*, 276, 1527–1530, doi:10.1126/science.276.5318.1527.
- Thompson, T. W., E. A. Ustinov, and E. Heggy (2008), Modeling radar scattering from icy lunar regoliths. *Lunar Planet. Sci.*, XXXIX, abstract 1023.
- Vasavada, A. R., D. A. Paige, and S. E. Wood (1999), Near-surface temperatures on Mercury and the Moon and the stability of polar ice deposits, *Icarus*, 141, 179–193, doi:10.1006/icar.1999.6175.
- Wilhelms, D. E. (1987), The Geologic History of the Moon, *U.S. Geol. Survey Prof.*, 1348, 302.
- S. M. Baloga, Proxemy Research Inc., 20528 Farcroft Lane, Laytonville MD 20882, USA.
- D. B. J. Bussey, D. Carl, M. Hillyard, R. Jensen, D. LaVallee, P. McKerracher, C. D. Neish, S. Nylund, W. Patterson, R. K. Raney, R. C. Schulze, H. Sequeira, J. Skura, B. J. Thomson, and H. L. Winters, Johns Hopkins University Applied Physics Laboratory, 11100 Johns Hopkins Rd., Laurel, MD 20723, USA.
- B. J. Butler, National Radio Astronomy Observatory, Socorro, NM 87801, USA.
- L. M. Carter, Center for Earth and Planetary Studies, Smithsonian Institution, Washington, DC 20013, USA.
- M. Chakraborty, Space Applications Centre, ISRO, Ahmedabad 380015, India.
- R. C. Elphic, Planetary Systems Branch, NASA Ames Research Center, MS 245-3, Moffett Field, CA 94035, USA.
- J. J. Gillis-Davis, Hawaii Institute of Geophysics and Planetology, University of Hawaii, Post 504, 2525 Correa Rd., Honolulu, HI 96822, USA.
- J. N. Goswami, Physical Research Laboratory, Ahmedabad 380009, India.
- E. Heggy, T. W. Thompson, and E. A. Ustinov, Jet Propulsion Laboratory, 4800 Oak Grove Dr., MS 300-227, Pasadena, CA 91109, USA.
- R. L. Kirk, Astrogeology Program, U.S. Geological Survey, 2255 N. Gemini Dr., Flagstaff, AZ 86001, USA.
- M. Palsetia, Vexcel Inc., 5775 Flatiron Pkwy., Suite 220, Boulder, CO 80301, USA.
- S. Nozette and P. D. Spudis, Lunar and Planetary Institute, 3600 Bay Area Blvd., Houston, TX 77058, USA. (spudis@lpi.usra.edu)
- M. S. Robinson, School of Earth and Space Exploration, Arizona State University, Box 871404, Tempe, AZ 85287, USA.